Robotic Irrigation Water Management: Estimating Soil Moisture Content by Feel and Appearance

Marsela Polic, Marko Car, Jelena Tabak and Matko Orsag

Abstract— In this paper we propose a robotic system for Irrigation Water Management (IWM) in a structured robotic greenhouse environment. A commercially available robotic manipulator is equipped with an RGB-D camera and a soil moisture sensor. The two are used to automate the procedure known as "feel and appearance method", which is a way of monitoring soil moisture to determine when to irrigate and how much water to apply. We develop a compliant force control framework that enables the robot to insert the soil moisture sensor in the sensitive plant root zone of the soil, without harming the plant. RGB-D camera is used to roughly estimate the soil surface, in order to plan the soil sampling approach. Used together with the developed adaptive force control algorithm, the camera enables the robot to sample the soil without knowing the exact soil stiffness a priori. Finally, we postulate a deep learning based approach to utilize the camera to visually assess the soil health and moisture content.

I. Introduction

The recent rise of robots in agriculture includes various application, ranging from picking [1], pruning [2], pollination [3] etc. However, taking care of the plant includes maintaining the health of the soil in which it grows. The *feel and appearance method* is actually a well defined and proscribed procedure farmers use to schedule irrigation of their crops [4]. It is a way of monitoring soil moisture to determine when to irrigate and how much water to apply. It is a common knowledge that plants need water to live and grow. However, applying too much water wastes this precious resource, and causes the loss of nutrients available for the plant. The feel and appearance of soil vary with texture and moisture content. Experienced farmers can estimate soil moisture conditions, to an accuracy of about 5 percent. Even though it is best to vary the number of sample sites and depths according to crop, field size, soil texture, and soil stratification, unfortunately to save time and effort the soil is typically sampled at three or more sites per field. For each sample the "feel and appearance method" involves various steps of tactile and visual inspection, comparing observations with photographs and/or charts to estimate percentage of the available water.

One of the goals within the SpECULARIA project [5] is to automate procedures like this, reducing human labor input in small indoor farms by replacing it with a heterogeneous team of robots. This team of robots is used in structured greenhouse cultivation, where plants are grown in container units so that they can be transported around the greenhouse by an unmanned ground vehicle (UGV). The UGV transports

Authors are with Faculty of Electrical Engineering and Computing, University of Zagreb, Unska 3, 10000 Zagreb, Croatia `marsela.polic, marko.car, jelena.tabak, matko.orsag @fer.hr`

Fig. 1: Collaborative robot Franka Panda performing soil moisture measurement procedure on a sweet pepper (Capsicum anuum) plant with a smart IoT moisture sensor.

the plants to the workstation, where a robotic manipulator treats the plants under controlled conditions. The structure of the controlled workspace around the robot gives it an upper hand when compared to mobile robots that manipulate plants in various conditions all over the farm. This paper focuses on the adaptive compliant control algorithm that enables the robot to sample the soil around the sensitive parts of the plant, and measure the water content close to the root of the plant. The method allows manipulation of objects of variable and unknown stiffness, ranging from manipulation of soft, wet ground, to handling collisions with rigid object such as roots or stones. The collaborative manipulator, which is the focus of this paper, is equipped with an RGB-D camera and a soil moisture sensor. The camera is used to estimate the position of the soil in the pot. Even though a rough estimate of the soil surface can be known a priori, the exact position varies during the entire vegetation process, as well as across the plant containers. Furthermore, the compliant control method additionally provides an estimate of the equivalent stiffness of the soil, thus providing another characteristic of the considered soil that can be used for describing the conditions. Combining different modalities will ultimately enable us to derive an AI based Expert system capable of soil moisture condition estimation utilized to plan optimal irrigation strategies for the greenhouse.

II. Related work

The work presented here relies on a widespread IoT solution for soil moisture measurement. The Soil Moisture Sensor utilizes a simple breakout for a straightforward method to measure water content in the soil [6]. The two exposed

pads function as probes acting as a variable resistor. The amount of water in the soil is reflected in the electrical conductivity between the pads, and is observed as a lower effective electrical resistance. The standard farming approach is to place the sensors and keep them in the ground for continuous measurements. Unfortunately, the exposed pads are quick to corrode, causing inconsistent measurements and harming the plants. Therefore, this sensor solution is recently being replaced with a more expensive versions of the soil moisture sensors. However, in the envisioned scenario we aim to utilize the existing resistance-based sensors, for two main reasons. First, such an end effector adapter is cost-effective, and the deployment with the robotic arm as opposed to fixed long-term measurements reduces the corrosion issue. The second motivation to use this type of sensor is in its physical resemblance to the U-fork, patented in France 1963, also known as the grelinette [7]. This tool is intended for soil aeration and drainage performed by digging the dirt around the plant to gently loosen it.

Inspired by the pioneering work of Hogan [8], impedance control of robotic manipulators has been extensively researched over the past decades, resulting in a development of a whole range of different impedance control strategies [9]. Impedance controllers have been applied for a wide variety of tasks, including, but not limited to, robotic rehabilitation, industrial manipulation, micro-manipulation and agricultural grasping and picking [10]. It has been shown that both accurate force tracking and soft grasping can be achieved using impedance controller [11], [12], which has been successfully tested in agricultural applications as well [13], [14]. In [13], authors presented an impedance control strategy for compliant fruit and vegetable grasping, while an impedance-based compliant plant exploration framework has been presented in [14]. In this work, the classical impedance control is extended with an adaptive control law that enables the robot to sample the soil without a priori knowing its exact stiffness.

To enable the adaptation law to estimate the stiffness of the ground, however, prior to placing the sensor in the ground, it is necessary to estimate the exact position of the soil surface inside the pot. Common approaches to the plane detection problem include computing surface normals and using standard Random Sample Consensus (RANSAC) algorithm [15], or its improved, noise-resistant version [16], on the point cloud obtained with an RGB-D camera. Alternative approaches are based on region growing methods [17] and Hugh transform [18], or a combination of both [19]. The approach proposed in this work uses the high performing RANSAC algorithm and addresses the problem of spurious planes by fitting the plane model only on the subset of the point cloud extracted with the custom ground plane detection method. This custom ground plane detection uses the existing information about the structured conditions in which the plants are grown.

III. GROUND PLANE DETECTION

As the plant is watered while it grows over a period of time, the surface of the ground surrounding the plant tends to gradually drop. This adds to the uncertainty of the motion control parameters. Even though a rough estimate of the surface of the soil can be assumed from the structured nature of the greenhouse and the plant containers, knowing the precise position of the surface allows for commanding the compliant control motion with a predetermined force, and using the adaptive control strategy to estimate the stiffness of the ground. The ground plane was detected using information from a consumer RGB-D camera, Intel RealSense D435, which was mounted on the manipulator in an *eye-in-hand* configuration. The camera calibration procedure was conducted in an autonomous manner, as described in [20], yielding the transformation between the camera (L_c) and the flange (L_f) where the camera is mounted $\mathbf{T}_f^c \in \mathbb{R}^{4 \times 4}$.

The obtained camera-flange transformation, along with the known robot kinematics $\mathbf{T}_0^f(\mathbf{q})$, is used to transform the point cloud measurments $\boldsymbol{\pi}_i$ from the local camera frame to the global reference frame $\mathbf{p}_i = \mathbf{T}_0^f(\mathbf{q}) \cdot \mathbf{T}_f^c \cdot \boldsymbol{\pi}_i$. Here we used L_0 to denote the base frame, and $\mathbf{q} \in \mathbf{R}^n$ to denote the n joints of the robot. For clarity we assume mapping between homogenoeus and Cartesian space is done implicitly when using vectors. Once the point cloud is transformed, NaN values and points which are out of the robot reach are filtered. As the robot is operating within the structured environment, the z coordinate of the table top position z_{TT}, on which the pot is placed, as well as the height of the pot z_{pot}, is known a priori, enabling us to filter points $\mathbf{p}_i \cdot \hat{\mathbf{z}}_0 < z_{TT}$ and $\mathbf{p}_i \cdot \hat{\mathbf{z}}_0 > z_{TT} + z_{pot} + \epsilon$. $\hat{\mathbf{z}}_0$ denotes the z axis of the base frame L_0. Finally, the remaining set of points $\mathbb{E}_0$ in the reachable environment of the robot is defined as:

$$
\begin{aligned}
\mathbb{E}_0 = \{ \mathbf{p} \in \{\mathbb{PC}\} | & x_{min} < x_p < x_{max}, \\
& y_p < y_{max}, \\
& z_{TT} < z_p < z_{TT} + z_{pot} + \epsilon \},
\end{aligned}
\tag{1}
$$

where the point $\mathbf{p}$ from the point cloud $\mathbb{PC}$ belongs to the set of points $\mathbb{E}_0$ if it is within the robot reach and if its z coordinate is bigger than the z_{TT} and smaller than the sum of z_{TT} and z_{pot}, increased by the small positive value ϵ. The set of points $\mathbb{E}_0$ is sorted based on the ascending z value.

The points from the set $\mathbb{E}_0$ are split into bins based on their z coordinates with the initial Δz being set to $7cm$. Score for each bin is calculated according to the set of equations 2.

$$
\begin{aligned}
s1 &= \frac{||B_{c-1}| - |B_c||}{|B_{c-1}| + |B_c| + 1} \cdot |B_c| \\
s2 &= \frac{||B_c| - |B_{c+1}||}{|B_c| + |B_{c+1}| + 1} \cdot |B_c| \\
s &= \frac{s1 + s2}{2},
\end{aligned}
\tag{2}
$$

where $|B_c|$ denotes the number of points in the current bin for which the score **s** is being calculated. The calculated score represents the number of points in the current bin, scaled with the relative difference between the number of points in the
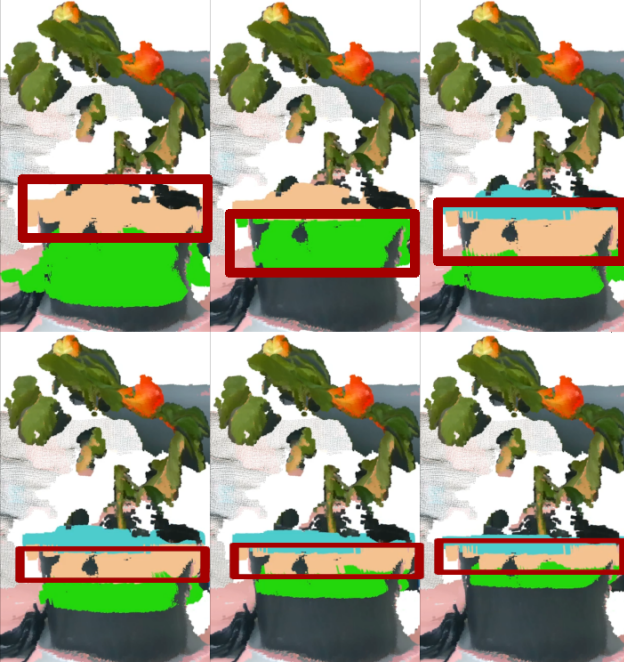
Fig. 2: The ground plane is segmented by iteratively dividing the subset of points into bins, shown in different colors, and selecting the highest scoring bin (denoted with red rectangle).
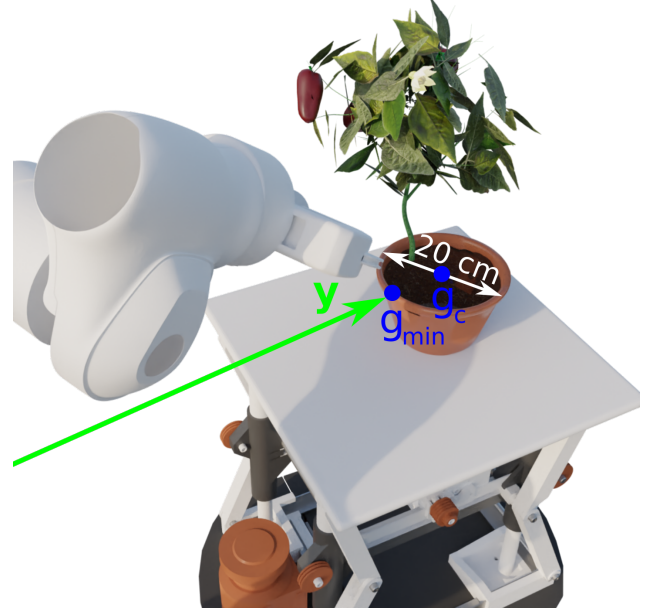

Fig. 3: Blender setup for validation of the soil surface detection method. The simulated RGB-D camera records a realistic pepper plant model grown in a container. Robot approach vector y is shown along with the ground truth point closest to the robot ($\mathbf{g}_{min}$) and ground truth center ($\mathbf{g}_c$).

current bin and the number of points in the neighbouring bins. It is expected that the bin with the highest score contains the points which belong to the ground plane. After selecting the highest scoring bin, the set of points $\mathbb{E}_k$ is updated as in Eq. 3:

$$\mathbb{E}_k = \{\mathbf{p} \in \{\mathbb{E}_{k-1}\} | (z_{b_{min}} - \frac{\Delta z}{2}) < z_p < (z_{b_{max}} + \frac{\Delta z}{2})\},$$
(3)

where $z_{b_{min}}$ and $z_{b_{max}}$ stand for the minimum and the maximum value of the z coordinates of the points in the highest scoring bin, respectively. After each iteration, the value of Δz is reduced by 25%. The algorithm is terminated once the value of Δz decreases to $1cm$. The visualization of the bins throughout the single experiment is shown in Fig. 2.

Plane model is fitted on the remaining $\mathbb{E}_k$ set of points using open sourced Point Cloud Library [21] implementation of the RANSAC algorithm [22]. The center of the ground plane $\mathbf{g}_c$ is defined as the median value across all three coordinates of the plane inliers and the point closest to the robot $\mathbf{g}_{min}$ is obtained by replacing the y value of the $\mathbf{g}_c$ with the minimum value of the y coordinates of the plane inliers.

Prior to conducting an experimental validation, the proposed method is validated in the simulation environment. Custom pepper plant models were generated for simulation validation, along with the plastic growth container and the soil surface inside it. The soil surface was modelled with variation along the z axis for a more realistic morphology. In the simulation environment, RGB and depth images of pepper

plants are generated using 3D modeling software, Blender [23]. The generated images served as an input to the custom ROS package, *blender_rgbd_ros* [24], which converts them to the point cloud data and publishes both images and point clouds on separate ROS topics. Camera intrinsic parameters used for image generation correspond to the parameters of the camera used in the real experiments, Intel RealSense D435.

Blender setup is shown in Fig. 3. As in the real environment, y axis of the reference coordinate system points towards the plant container. In the simulation environment, the exact position of $\mathbf{g}_c$ and $\mathbf{g}_{min}$ can easily be extracted, enabling the accurate comparison of the estimates and the ground truth. Both the mean value and the standard deviation of the soil surface estimates for a single plant recorded from 10 random positions, along with the ground truth value, are shown in Table I. The error and the dissipation of the x_{median}, y_{median} and y_{min} are at a millimeter level, meaning that, even in the worst case scenario, estimated ground center lies within the close environment of the ground truth center, as can be seen in Fig. 4. The dissipation of the z estimate, z_{median}, is even smaller, which was expected, considering that the plane model was fitted on the modeled surface plane points, which differed in the value of their z coordinate for up to $1cm$. The error and the dissipation of the z estimate are sufficiently small for the successful implementation of the adaptive compliant control strategy. Knowing the central position of the soil with respect to the plant enables the robot to sample at the safe distance from plant's sensitive roots.

TABLE I: Ground truth and soil surface estimates in the simulation environment for the single plant recorded from 10 random positions. Diameter of the top of the pot is $20cm$.

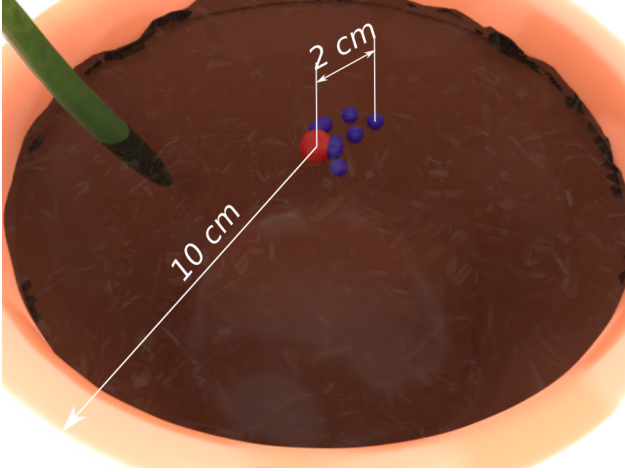|	ground truth	mean	std
x_{median} [mm]	1.8	3.4	6.8
y_{median} [mm]	0.8	4.0	5.0
y_{min} [mm]	-100	-96.2	3.8
z_{median} [mm]	110.2	111.2	0.1

Fig. 4: Visualization of the ground center estimates of the soil surface modeled in Blender. Red sphere denotes the ground truth center and the blue spheres denote the estimates for each of the 10 experiment repetitions. The radius of the modeled pot is $10cm$ and the maximum distance between the ground truth and the estimate is $2cm$. Texture of the soil surface is semi-transparent for the better visualization.

IV. ADAPTIVE COMPLIANT CONTROL

In this work, interaction of the end-effector with the environment relies on impedance control in the Cartesian space. The impedance filter models the robot-environment interaction system with an equivalent spring. The force tracking error between the desired contact force $\mathbf{F}_r$ and the measured force $\mathbf{F}$ as in eq. 4, drives robot motion according to the desired mass-spring-damper system properties.

$$\mathbf{E} = \mathbf{F}_r - \mathbf{F}. \quad (4)$$

Here we consider force control along three spatial axes, so that all the vectors used are from $R^{3\times 1}$. The user-defined target impedance behavior of the system determines the dynamic relationship between the robot position and the force tracking error so that it mimics a mass-spring-damper system as in eq. 5,

$$\mathbf{E} = \mathbf{M}(\ddot{\mathbf{X}}_c - \ddot{\mathbf{X}}_r) + \mathbf{B}(\dot{\mathbf{X}}_c - \dot{\mathbf{X}}_r) + \mathbf{K}(\mathbf{X}_c - \mathbf{X}_r), \quad (5)$$

where $\mathbf{X}_c$ and $\mathbf{X}_r$ are $R^{3\times 1}$ commanded and reference position vectors of the end-effector, and $\mathbf{M}$, $\mathbf{B}$ and $\mathbf{K}$ are the $R^{3\times n}$ mass, damping and stiffness matrices of the target impedance, respectively. The reference position is the one provided by the user or by a higher level control. The commanded position is the actual input reference for the robot Cartesian position control. When in contact with the environment, the commanded robot position $\mathbf{X}_c$ changes with the measured contact force through eq. 5, and the position tracking is in general not accurate. In other words, the impedance filter balances the position and force tracking errors. Switching to analysis along a single spatial axis without loss of generality, it can be shown [25] that the desired contact forces can only be realized in case both precise environment position and the environment equivalent stiffness are known, by generating an adequate position reference x_r using eq. 6

$$x_r = \frac{F_r}{k_e} + x_e, \quad (6)$$

where F_r is the desired contact force, and k_e and x_e are the environment stiffness and position, respectively. However, in the case presented in this work, the soil stiffness is unknown a-priori, and varies with the soil moisture. The controller used in this work is an extension of the classic position based impedance controller developed in [?], with online adaptation of the impedance filter inputs based on the estimated environment stiffness. The adaptation law for the position reference is based on the adaptive parameter $\kappa(t)$ that accounts for unknown elastic properties of environment under external force,

$$x_r(t) = \kappa(t)F_r + x_e, \quad (7)$$

where the position reference is a function of the estimate of the initial position of the environment x_e and the force reference F_r. The exact adaptation law is given with eq. 8 for one spatial dimension,

$$k\dot{\kappa}(t) + b\ddot{\kappa}(t) + m\dddot{\kappa}(t) = -\gamma_1 q(t) + \gamma_1^* \dot{q}(t),$$
$$q(t) = p_1 e(t) + p_2 \dot{e}(t) \quad (8)$$

where k, b, and m are the impedance filter parameters, $e(t)$ is the force tracking error, and p_1 and p_2 are the free parameters tuned based on the particular application. The derivation and convergence proof for this adaptation law can be found in [26]. The adaptation law 7 used for ensuring force reference tracking implicitly yields a stiffness estimate of the manipulated object. In this case, the soil stiffness measure is used both for compliant manipulation in moisture measurement, and as a feature in the proposed soil moisture monitoring framework.

V. EXPERIMENTAL VALIDATION

We conducted a series of experiments to verify how well the system estimates the position and the stiffness of the soil. In practice, the information gathered in such a way can help the system estimate the health of the soil and manage its water content.

A. Ground plane detection precision

In the same manner as in the simulation environment, a pepper plant was recorded from 10 random positions in the laboratory conditions. The center of the ground plane was estimated for each of the 10 frames as the median value of the

TABLE II: Dissipation of the estimates in the real environment for the single plant recorded from 10 random positions. Diameter of the top of the pot is $20cm$.

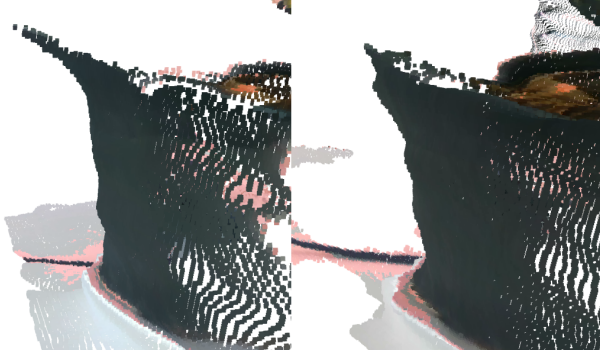|	x_{median}	y_{median}	y_{min}	z_{median}
Δ_{max} [mm]	26.3	46.6	26.1	5.0
std [mm]	8.7	13.6	7.3	1.5

Fig. 5: Erroneous point cloud of pot recorded with Intel RealSense D435.

fitted plane inliers across all three dimensions. The maximum difference and the dissipation of the estimates are shown in Table II. While the estimated value of z coordinate of the ground center remained sufficiently small and robust to the change in the camera recording angle, the estimated x and y values significantly deteriorated compared to the simulation environment. This can be explained by the imperfections of the depth module of the RealSense camera. An example of an inaccurate point cloud of pot is shown in Fig 5. This problem was addressed by extracting the closest point along the y coordinate on the detected plane with respect to the robot base, instead of the median value. The final y coordinate of the reference position is defined as $3cm$ further along the y coordinate, in order to reach the soil instead of the pot edge. As visible from the Table II, the dissipation is smaller when working with the y_{min} instead of y_{median}. This was not the case in the simulation environment, as the camera model simulated in Blender did not incorporate the fluctuations in the depth data. However, considering that the diameter of the top of the pot is equal to $20cm$, dissipation in both x and y values, though bigger than in the simulation environment, is still negligible.

B. Control

Soil sampling experiments were conducted with a Franka Panda collaborative robot arm, based on the described soil surface detection using impedance control methods. The experiments were conducted in three scenarios analyzing the framework behavior with respect to different soil conditions. The moist soil conditions represent the softest scenario, i.e. the least stiff environment if considering the estimated stiffness values. The dry soil conditions represent a stiff scenario, while the extreme was tested through collision with a very rigid object, representing e.g. a stone in the soil that could

potentially break the sensory equipment, or a part of the root system that should not be harmed. Five experimental repetitions were conducted for the first two scenarios, and three repetitions for the collision scenario. The results are represented in the graphs in figures 6b-7c.

The force responses in the figures 6b-6c are obtained with the same impedance filter, and the same parameters of the adaptation controller. The results show that the adaption in the framework is capable of reaching the desired contact force setpoint regardless of the stiffness of the manipulated object. When considering the responses, it should be noted that instead of a precise external force/torque sensor, the measurement is provided by the Franka Panda dynamics estimation model. The imprecision in the model can be observed particularly in the variable baseline offset in the measurements at the beginning and at the end of each experiment. Here, the robot is not in contact with the environment, and there are no external forces acting on the end-effector. However, the estimated forces are non-zero due to model imprecision, and vary depending on the robot pose and velocity.

The adaptation framework implicitly models the stiffness of the manipulated object, as shown in 6b-6c. Instead of the estimated stiffness, the responses show the dynamics of the inverse variable $1/K_e$, that could be considered compliance of the manipulated object (soil). For safety reasons, the initial assumption is that the manipulated object is infinitely stiff (zero compliance), and the adaptation of the estimated stiffness gradually reaches the actual value along with the desired contact forces. This is one of the reasons behind faster adaptation for a stiffer object, the other being the chosen adaptation parameters. These parameters would, in case of very compliant objects, probably have to be tuned for more aggressive (faster) adaptation. The compliance (stiffness) measure not only models the soil, but inherently takes into account the elasticity of the robot manipulator, as well as the imprecision of the soil surface detection. Regardless, the results show that throughout the repetitions, the estimation converges to the same region of values, proving the adaptation method is stable with respect to robot dynamics and detection imprecision.

VI. DISCUSSION

This paper presents a soil moisture measurement method and its experimental validation applicable for robotic plant cultivation. The detection method in the initial step relies on an RGB-D visual setup for detection of the soil surface within the container. Instead of relying on color based segmentation, which is sensitive with respect to the lighting and other external conditions, or on other complex segmentation techniques such as CNNs, the method relies on an iterative 3D pointcloud segmentation and RANSAC based plane fitting. The method validation in simulation was confirmed in experiments with real plants, showing that the method is suitable for detection of soil plane inside the growth container.

The actual measurement method relies on compliant control framework for a collaborative robot, that can easily be
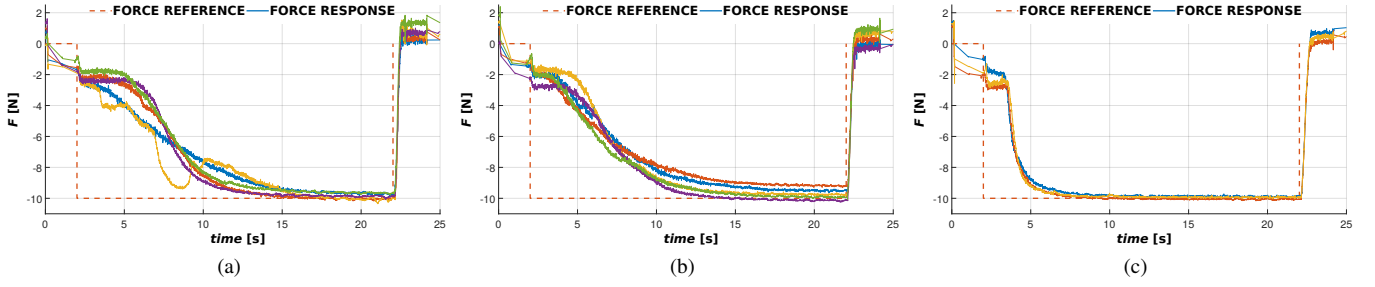
Fig. 6: Force tracking of the robot end effector in experiments on the softest object, moist soil 6a, on the stiffer object, namely dry soil 6b, and in case of collision with a rigid object 6c. The robot motion is safe for the manipulated objects regardless of their stiffness.
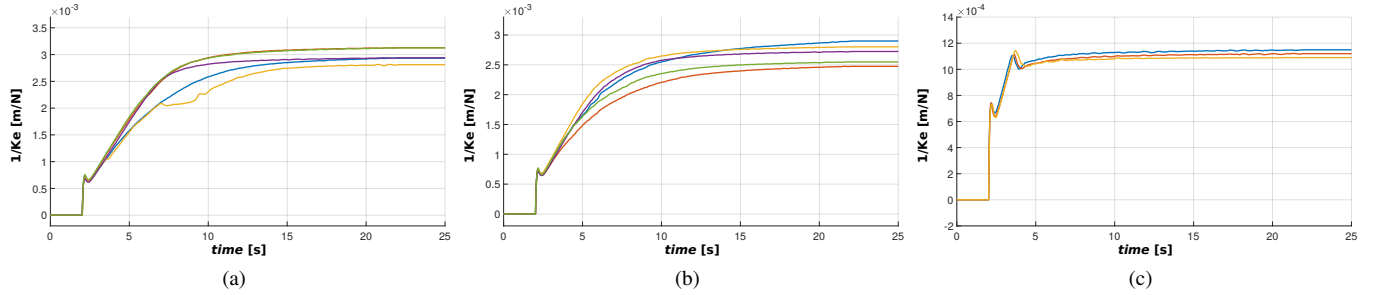

Fig. 7: Adaptation dynamics during experiments with moist soil 7a, dry soil 7b, and in case of collision with a rigid object 7c. The estimation also compensates manipulator dynamics and surface detection pipeline. Adaptation tuned for fastest convergence on stiffest objects.

applied to industrial manipulator equipped with an external force torque sensor as well. The method enables compliant manipulator control during interaction with a deformable fragile objects, without prior information on the mechanical properties. Moreover, the method implicitly models them during motion control in attempt to reach the desired contact force setpoint. However, the obtained compliance measure not only models the soil but other system components as well, such as manipulator dynamics, and the error in soil surface estimation, which explains the variation in the estimations obtained over experiment repetitions. Even though not converging to precisely the same value over several experiment repetitions, the estimates of the compliance measures for three tested scenarios still distinguish between various manipulation conditions, and imply that such a measure could be used as a part of the feel and appearance method. Most importantly, the method is shown suitable and safe both for the robot, and for the underground plant parts, on a variety of soil conditions ranging from the soft moist soil to stiff soils with rigid debris in an autonomous manner without additional pre-tuning.

In the final setup, the visual part of the "feel and appearance method" will be achieved using the equipped RGB-D camera. Combining all three modalities (i.e. vision, measured resistance and stiffness) will enable us to derive an AI based Expert system capable of estimating soil moisture conditions to plan optimal irrigation strategies for the greenhouse.

ACKNOWLEDGMENT

REFERENCES

[1] Y. Xiong, Y. Ge, L. Grimstad, and P. J. From, "An autonomous strawberry-harvesting robot: Design, development, integration, and field evaluation," *Journal of Field Robotics*, vol. 37, no. 2, pp. 202–224, 2020.

[2] Q. Zhang, M. Karkee, and A. Tabb, "The use of agricultural robots in orchard management," in *Robotics and automation for improving agriculture* (J. Billingsley, ed.), Burleigh Dodds Science Publishing, 2019.

[3] J. Strader, C. Yang, Y. Gu, J. Nguyen, C. Tatsch, Y. Du, K. Lassak, B. Buzzo, R. Watson, H. Cerbone, and N. Ohi, "Flower interaction subsystem for a precision pollination robot," pp. 5534–5541, 11 2019.

[4] N. L. Klocke and P. E. Fischbach, "G84-690 estimating soil moisture by appearance and feel," 1984.

[5] M. Polic, A. Ivanovic, B. Maric, B. Arbanas, J. Tabak, and M. Orsag, "Structured ecological cultivation with autonomous robots in indoor agriculture," in *2021 16th International Conference on Telecommunications (ConTEL)*, pp. 189–195, 2021.

[6] M. Saleh, I. H. Elhajj, D. Asmar, I. Bashour, and S. Kidess, "Experimental evaluation of low-cost resistive soil moisture sensors," in *2016 IEEE International Multidisciplinary Conference on Engineering Technology (IMCET)*, pp. 179–184, IEEE, 2016.

[7] K. Farhat, "Digging fork device for at least one digging fork," WO/2014/154983.

[8] N. Hogan, "Impedance control: An approach to manipulation," in *1984 American Control Conference*, pp. 304–313, 1984.

[9] H. Al-Shuka, S. Leonhardt, W.-H. Zhu, R. Song, C. Ding, and Y. Li, "Active impedance control of bioinspired motion robotic manipulators: An overview," *Applied Bionics and Biomechanics*, 06 2018.

[10] P. Song, Y. Yu, and X. Zhang, "A tutorial survey and comparison of impedance control on robotic manipulation," *Robotica*, vol. 37, pp. 1–36, 01 2019.

[11] Z. Ting, L. Jiang, S. Fan, X. Wu, and W. Feng, "Development and experimental evaluation of multi-fingered robot hand with adaptive impedance control for unknown environment grasping," *Robotica*, vol. -1, pp. 1–18, 08 2014.

[12] Y. Sano, R. Hori, and T. Yabuta, "Comparison between admittance and impedance control method of a finger-arm robot during grasping object with internal and external impedance control," *Transactions of the Japan Society of Machanical Engineers Series C*, vol. 79, pp. 4330–4334, 11 2013.

[13] X. Wang, Y. Xiao, S. Bi, X. Fan, and H. Rao, "Design of test platform for robot flexible grasping and grasping force tracking impedance control," *Nongye Gongcheng Xuebao/Transactions of the Chinese Society of Agricultural Engineering*, vol. 31, pp. 58–63, 01 2015.

[14] M. Polic, M. Car, F. Petric, and M. Orsag, "Compliant plant exploration for agricultural procedures with a collaborative robot," *IEEE Robotics and Automation Letters*, vol. 6, no. 2, pp. 2768–2774, 2021.

[15] D. Holz, S. Holzer, R. B. Rusu, and S. Behnke, "Real-time plane segmentation using rgb-d cameras," in *RoboCup 2011: Robot Soccer World Cup XV* (T. Röfer, N. M. Mayer, J. Savage, and U. Saranlı, eds.), (Berlin, Heidelberg), pp. 306–317, Springer Berlin Heidelberg, 2012.

[16] L. Li, F. Yang, H. Zhu, D. Li, Y. Li, and L. Tang, "An improved ransac for 3d point cloud plane segmentation based on normal distribution transformation cells," *Remote Sensing*, vol. 9, no. 5, 2017.

[17] A.-V. Vo, L. Truong-Hong, D. F. Laefer, and M. Bertolotto, "Octree-based region growing for point cloud segmentation," *ISPRS Journal of Photogrammetry and Remote Sensing*, vol. 104, pp. 88–100, 2015.

[18] R. Hulik, M. Spanel, P. Smrz, and Z. Materna, "Continuous plane detection in point-cloud data based on 3d hough transform," *Journal of Visual Communication and Image Representation*, vol. 25, no. 1, pp. 86–97, 2014. Visual Understanding and Applications with RGB-D Cameras.

[19] X. Leng, J. Xiao, and Y. Wang, "A multi-scale plane-detection method based on the hough transform and region growing," *The Photogrammetric Record*, vol. 31, pp. 166–192, 06 2016.

[20] B. Maric, M. Polic, T. Tabak, and M. Orsag, "Unsupervised optimization approach to in situ calibration of collaborative human-robot interaction tools," in *2020 IEEE International Conference on Multisensor Fusion and Integration for Intelligent Systems (MFI)*, pp. 255–262, IEEE, 2020.

[21] R. B. Rusu and S. Cousins, "3D is here: Point Cloud Library (PCL)," in *IEEE International Conference on Robotics and Automation (ICRA)*, (Shanghai, China), IEEE, May 9-13 2011.

[22] M. A. Fischler and R. C. Bolles, "Random sample consensus: a paradigm for model fitting with applications to image analysis and automated cartography," *Commun. ACM*, vol. 24, pp. 381–395, 1981.

[23] R. Hess, *Blender Foundations: The Essential Guide to Learning Blender 2.6*. Focal Press, 2010.

[24] A. Ivanovic, "blender_rgbd_ros." https://github.com/larics/blender_rgbd_ros, 2021. Accessed: 2021-10-10.

[25] H. Seraji and R. Colbaugh, "Force tracking in impedance control," in *[1993] Proceedings IEEE International Conference on Robotics and Automation*, pp. 499–506, IEEE Comput. Soc. Press.

[26] L. Marković, M. Car, M. Orsag, and S. Bogdan, "Adaptive stiffness estimation impedance control for achieving sustained contact in aerial manipulation," in *2021 IEEE International Conference on Robotics and Automation (ICRA)*, pp. 117–123, IEEE, 2021.

[27] M. Orsag *et al.*, "Specularia." https://sites.google.com/view/specularia-pepper-picking, 2021. Accessed: 2021-03-31.